11th International Symposium on Turbulence and Shear Flow Phenomena (TSFP11)
Southampton, UK, July 30 to August 2, 2019

NUMERICAL INVESTIGATION ON SCALE-BY-SCALE REYNOLDS STRESS TRANSPORT IN PLANE COUETTE TURBULENCE

Takuya Kawata
Department of Mechanical Engineering
Tokyo University of Science
2641 Yamazaki, Noda, 278-8510 Chiba, Japan
email: kawata@rs.tus.ac.jp

Takahiro Tsukahara
Department of Mechanical Engineering
Tokyo University of Science
2641 Yamazaki, Noda, 278-8510 Chiba, Japan
email: tsuka@rs.tus.ac.jp

ABSTRACT

Scale-by-scale Reynolds stress transport in a turbulent plane Couette flow is investigated by means of direct numerical simulation. For reducing computational cost, we employ a computational domain whose spanwise length is large enough to capture the essential dynamics of the flow whereas the streamwise extent is as small as the minimal length. The computation with such a reduced-size domain is confirmed to well reproduce the statistical characteristics of the flow including the spectral contents. We investigate the spectral budget of the Reynolds-shear-stress transport with a particular interest in the roles of the interscale and spatial transport by nonlinear scale interactions, and the effect of pressure, which is extremely difficult to measure by experiment, is also discussed.

INTRODICTION

With the significant advances in experimental techniques and high-performance computation in recent years, there have been overwhelming evidences showing that in wall turbulence there exist very-large-scale structures away from the wall and they become increasingly energetic with the increasing Reynolds number (see, for example, Smits *et al.*, 2011, and the references therein). In particular, recent experimental data from high-Reynolds-number facilities such as the Prinston Superpipe and the CICLoPE facility at the University of Bologna have clearly shown the emergence of the outer peak of the streamwise velocity fluctuation at very high Reynolds numbers (Hultmark *et al.*, 2012; Willert *et al.*, 2017; Samie *et al.*, 2018), indicating that the large-scale structures may play further important role in wall turbulence at higher Reynolds numbers.

Such observations on the very-large-scale structures have also raised the interest in their influences over the smaller-scale structures in the near-wall region. Earlier studies on such top-down effect from outer to inner regions have been mainly motivated by the failure of the viscous scaling of the near-wall behaviour of wall turbulence. Hutchins & Marusic (2007) indicated that the amplitude of small-scale events in the near-wall region is modulated by the large-scale structures in the outer region, and the degree of such interaction becomes more significant at higher Reynolds numbers. Such inner-outer interaction is often referred to as the amplitude modulation, and there have been many discussions on the subject, as summarised by Dogan *et al.* (2018).

From the view point of the Reynolds stress transport, such interaction between the structures with different scales at different wall-normal positions may be expressed as interscale and/or spatial transport of the Reynolds stresses. Such scale-by-scale analysis of turbulence transport has been performed in earlier studies based on different turbulent statistical quantities such as turbulent energy spectra (Lee & Moser, 2017; Mizuno, 2016) and the second-order structure function (Cimarelli *et al.*, 2016). Among these recent analyses, Kawata & Alfredsson (2018) showed that the Reynolds shear stress is transferred from smaller to larger scales throughout the channel, and the contribution by the interscale and spatial transports can be viewed as the influence from the small-scale near-wall structures to the very-large-scale structures in the outer region. However, they did not investigate all the terms in the transport equation. In particular, the behaviour of the pressure-related terms at each scale has still not been unveiled.

In the present study, we perform direct numerical simulation (DNS) of a turbulent plane Couette flow. In this flow very-large-scale vortical structures appear in the channel core region even at moderate Reynolds numbers (for example, Lee & Kim, 1991; Bech *et al.*, 1995; Komminaho *et al.*, 1996), and through the interscale and spatial transport of the Reynolds stress the influence from the near-wall to large-scale structures can be observed. Our analysis follows the procedure by Mizuno (2016), and all terms of the scale-by-scale Reynolds-stress equations are evaluated. The roles of interscale and spatial turbulent transport and the pressure-related terms are mainly discussed in details.

Table 1. Computational conditions: domain size, number of grid points in each direction. The Reynolds number Re_w and the time step are $Re_\mathrm{w} = 8600$ and $\Delta t^* = 0.004$, respectively. The obtained values of the friction Reynolds number Re_τ, domain size and spatial resolution in terms of the wall units are also given.

	L_x, L_z	$N_x \times N_y \times N_z$	Re_τ	L_x^+, L_z^+	Δx^+, Δz^+	Δy^+
Lx-96	$96h$, $12.8h$	$2048 \times 96 \times 512$	126.2	24230, 3231	11.83, 6.31	0.18–5.66
Lx-24	$24h$, $12.8h$	$512 \times 96 \times 512$	125.8	6031, 3222	11.80, 6.29	0.26–6.14
Lx-6.4	$6.4h$, $12.8h$	$128 \times 96 \times 512$	126.7	1622, 3245	12.67, 6.34	0.26–6.19
Lx-1.6	$1.6h$, $12.8h$	$32 \times 96 \times 512$	126.8	406, 3248	12.68, 6.34	0.26–6.19

COMPUTATIONS

The plane Couette flow considered in the present study is defined by a stationary bottom wall and a top wall translating with a constant speed U_w. The spacing between the top and bottom walls is h, and x-, y-, and z-axes are taken in the streamwise, wall-normal, and spanwise directions with the origin of the coordinates fixed on the stationary bottom wall. The velocity components in theses directions are $\tilde{u} = U + u$, $\tilde{v} = V + v$, and $\tilde{w} = W + w$, where the upper- and lowercase letters without tilde represent the mean values and the deviations from them, respectively.

The governing equations for simulation are the non-dimensionalised continuity and Navier-Stokes equations for incompressible fluid:

$$\frac{\partial \tilde{u}_i^*}{\partial x_i^*} = 0 \tag{1}$$

$$\frac{\partial \tilde{u}_i^*}{\partial t^*} + \tilde{u}_j^* \frac{\partial \tilde{u}_i^*}{\partial x_j^*} = -\frac{\partial \tilde{p}^*}{\partial x_i^*} + \frac{1}{Re_\mathrm{w}} \frac{\partial^2 \tilde{u}_i^*}{\partial x_j^*} \tag{2}$$

where u_i, p, and t are the velocity, pressure, and time, and the superscript * in the equations above stands for the dimensionless quantities scaled by the wall velocity U_w and/or the channel gap h. Re_w is the Reynolds number based on h and U_w: $Re_\mathrm{w} = U_\mathrm{w} h/\nu$ (ν is the kinematic viscosity of the fluid), and in all computational runs in the present study we fix the Reynolds number at $Re_\mathrm{w} = 8600$.

The governing equations (1) and (2) are discretised by the central difference method: the second- and forth-order schemes are adopted for the wall-normal (y-) and the other directions, respectively. For time-advance algorithm, the second-order Crank-Nicolson method is adopted for the viscous term for the wall-normal direction, while the Adams-Bashforth method of the same order of accuracy is used for the other terms.

Earlier studies on the turbulent plane Couette flow showed that the typical streamwise wavelength of the very-large-scale structure in the core region is 20–30 times of the channel height (e.g. Tsukahara *et al.*, 2006; Avsarkisov *et al.*, 2015), indicating that it is required to use an extremely large computational domain in order to capture all the streamwise wavelengths involved in the dynamics. The computational cost for such 'full' DNS of the plane Couette flow is, therefore, usually quite heavy even at low Reynolds numbers. On the other hand, in some earlier studies a reduced-size computational domain was used, whose streamwise extent is as small as the minimal length, i.e. the least domain length to sustain the near-wall cycle, while the spanwise one is large enough to capture several pairs of large-scale structures (Toh & Itano, 2005; Abe *et al.*, 2018). In these studies, due to the massively reduced degree of freedom in the streamwise direction, the large-scale structures in the outer layer were forced to be streamwise two-dimensional, while the degree of freedom was retained for the near-wall structures in the inner layer. By using such a reduced-size domain, Toh & Itano (2005) 'simplified' the flow field of wall turbulence retaining both the inner- and outer-layer structures and investigated interaction between them. Abe *et al.* (2018) also demonstrated that the computation with such streamwise-minimal domain reproduce statistical characteristics of wall turbulence qualitatively well.

In the present study, we use a streamwise-reduced computational domain following aforementioned earlier studies for investigating interaction between the near-wall and large-scale structures in turbulent plane Couette flow with an affordable computational cost. In order to examine the effect of reducing streamwise domain size, several computations were run with different streamwise domain lengths, as summarised in Table 1. For all the computational runs the spanwise extent of the computational domain is $L_z = 12.8h$, which corresponds to about 6 pairs of the large-scale structures in the core region. The largest computational domain employed in this study has the streamwise extent of $L_x = 96h$ (Lx-96), while that of the smallest one (Lx-1.6) is $L_x = 1.6h$, which corresponds to about 400 wall units and is therefore as small as the streamwise minimal length (Jimenez & Moin, 1991).

RESULTS AND DISCUSSIONS

The effect of reducing domain size

The obtained values of the friction Reynolds number $Re_\tau = u_\tau \delta/\nu$ ($\delta = h/2$) and the domain size and spatial resolutions scaled by the wall units are also given in Table 1, and one can see here that reducing the streamwise domain extent does not significantly affect the obtained value of Re_τ. All the values of Re_τ shown in Table 1 are within ± 0.5 % of the values obtained in the Lx-96 case.

Figure 1 presents the profiles of the mean streamwise velocity and Reynolds stresses obtained with the different computational domains. As shown in Fig. 1(a) the mean velocity profiles obtained with different streamwise computational-domain-length are in a quite good agreement with each other, showing almost no influences of reducing the domain size. The Reynolds stress profiles given in Fig. 1(b) also show a qualitative agreement, while certain quantitative discrepancies are observed in the profiles of $\langle u^2 \rangle$ and $\langle w^2 \rangle$. The values of the streamwise normal stress $\langle u^2 \rangle$ in the streamwise-minimal case Lx-1.6 are slightly overestimated compared to those in the largest domain case Lx-96, while the spanwise component $\langle w^2 \rangle$ in the Lx-1.6 case is underestimated throughout the channel. It is note-

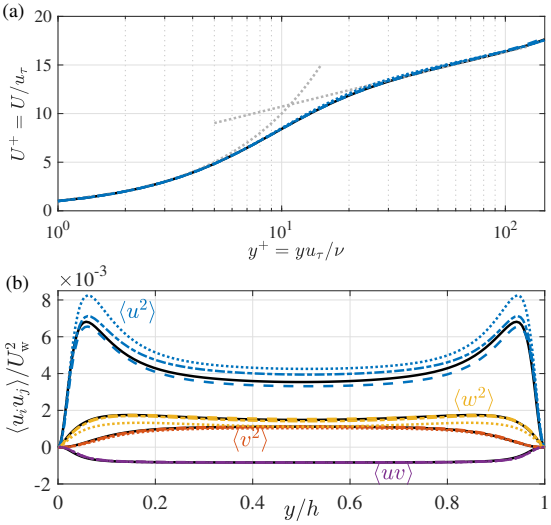

Figure 1. Profiles of (a) the mean streamwise velocity and (b) the Reynolds stresses obtained with different streamwise domain sizes. In both panel (a) and (b), the solid (——), dashed (− −), dash-dotted (− · −), and dotted (· · ·) line indicate the case Lx-96, Lx-24, Lx-6.4, and Lx-1.6, respectively. For readability of the figure, the results of the case Lx-96 is shown in black, while the other cases are shown in different colours: (a) all other cases are shown in blue; (b) the profiles of $\langle u^2 \rangle$, $\langle v^2 \rangle$, $\langle w^2 \rangle$, and $\langle uv \rangle$ are shown in blue, red, yellow, and purple, respectively.

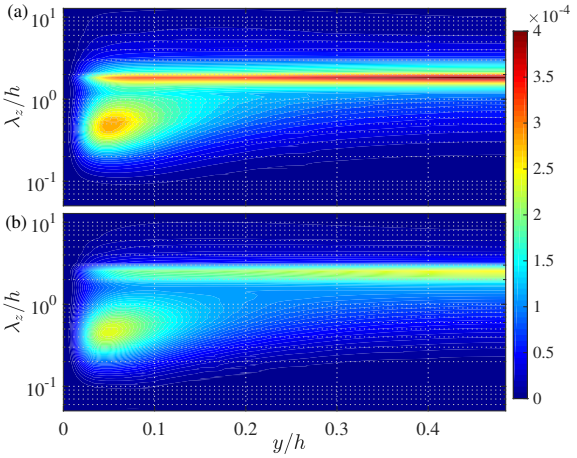

Figure 2. Distribution of spanwise one-dimensional spectra of streamwise velocity fluctuation E_{uu}: (a), Lx-1.6 (the streamwise-minimal case); (b) Lx-96. The values are scaled based on h and U_w.

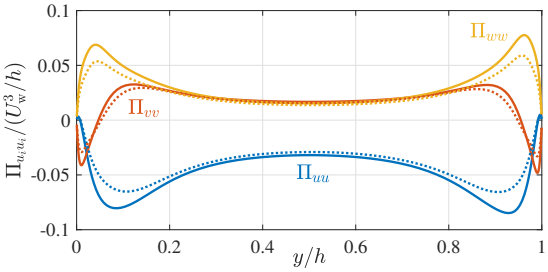

Figure 3. Profiles of the pressure-strain correlations obtained in (solid lines) the Lx-96 and (dotted lines) Lx-1.6 cases: blue, $\Pi_{uu} = -\langle p\partial u/\partial x \rangle$; red, $\Pi_{vv} = -\langle p\partial v/\partial y \rangle$; yellow, $\Pi_{ww} = -\langle p\partial w/\partial z \rangle$.

worthy that despite of such difference in the normal stress components the Reynolds shear stress $\langle uv \rangle$ is not affected by reducing domain size, which results in the good agreement in the obtained values of Re_τ in Table 1.

Figure 2 presents space-wavelength (y-λ_z) diagram of the spanwise spectra of the streamwise fluctuating velocity E_{uu}. One can see here that the distributions obtained in the Lx-1.6 and Lx-96 cases are in a good qualitative agreement: both results show a distinct energy band located at relatively large wavelengths around $\lambda_z \approx 2h$ ranging from the near-wall to the channel central region, which clearly corresponds to the large-scale structures in the channel core region. An energy peak is also found in the near-wall region at relatively small wavelength; corresponding to the near-wall region with typical spanwise scale about 100 wall units. The magnitude of the turbulent energy spectra is somewhat larger in the Lx-1.6 case than those in the Lx-96 case, corresponding to the $\langle u^2 \rangle$ values given in Fig. 1(b).

As described above, reducing the streamwise domain size to as small as the minimal length is shown to have an effect to overestimate the streamwise velocity fluctuation. Such an effect of reducing domain size on the Reynolds normal stresses can be explained by the Reynolds-stress redistribution by the pressure-strain correlation. As shown in Fig. 3 the redistribution term for the streamwise normal component $-\langle p\partial u/\partial x \rangle$ is suppressed in the streamwise-minimal case (Lx-1.6) compared to the Lx-96 case. This is attributable to the limited degree of freedom in the streamwise direction in the Lx-1.6 case that forces most of the vortical structures to be two-dimensional in the streamwise direction, i.e. $\partial u/\partial x \approx 0$. Corresponding to this, the spanwise component $-\langle p\partial w/\partial z \rangle$ is also suppressed in the Lx-1.6 case, indicating that the inter-component energy transfer between the streamwise and spanwise velocity fluctuations by the pressure-strain correlation is suppressed. On the other hand, similarly to the wall-normal velocity fluctuation $\langle v^2 \rangle$, the wall-normal component of the pressure-strain correlation $-\langle p\partial v/\partial y \rangle$ is relatively not affected by the change in the domain size.

Scale-by-scale Reynolds-stress transport

In this section, we investigate the scale-by-scale balance in the transport equation of turbulent kinetic energy and the Reynolds shear stress. The results of the streamwise-minimal case is used in the following scale-by-scale analysis and the scale decomposition is based on the spanwise Fourier modes. The scale-by-scale transport equation of the Reynolds stress is written as:

$$\frac{DE_{ij}}{Dt} = P_{ij} - \varepsilon_{ij} + \Phi_{ij} + D^\nu_{ij} + + N_{ij} \tag{3}$$

where $E_{ij}(k_z) = \Re\left(\overline{\hat{u}_i(k_z)\hat{u}_j(-k_z)}\right)$ is the spanwise Reynolds stress spectra, where the hat and over bar stand for the spanwise Fourier coefficient and the averaging operator in x-direction and in time, respectively, and $\Re$ indicates the real part of complex quantity. P_{ij}, ε_{ij}, Φ_{ij}, and D^ν_{ij} are the spectral component of the Reynolds-stress production,

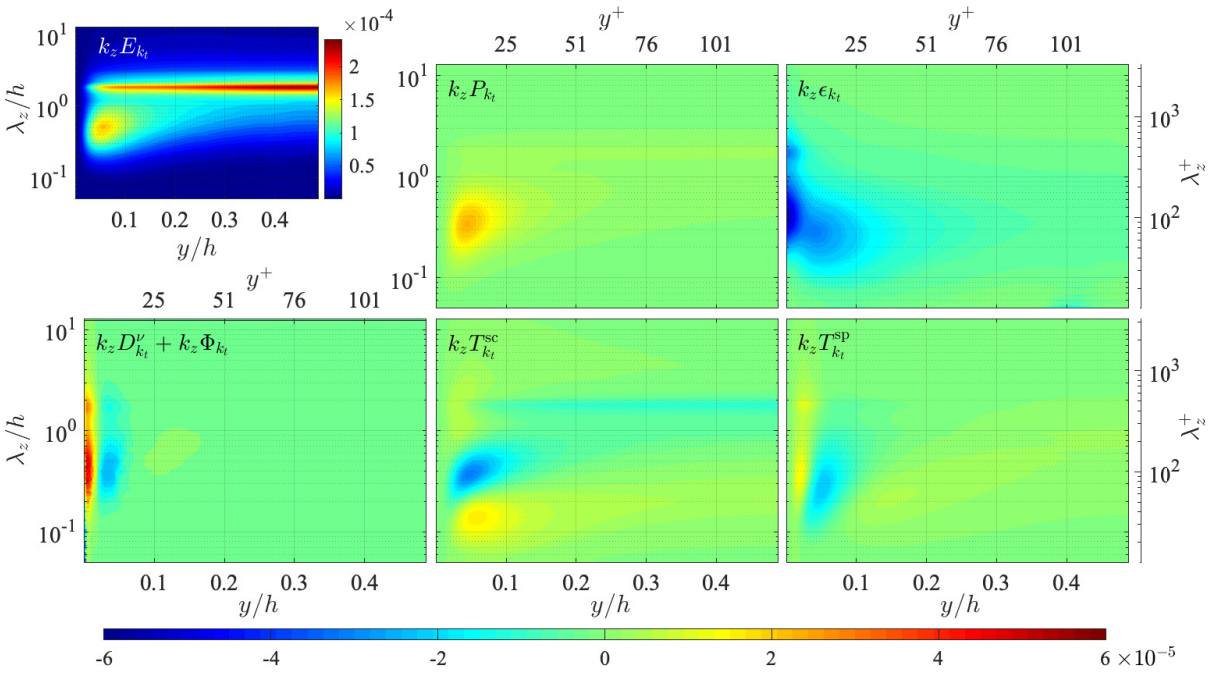

Figure 4. Space-wavelength (y-λ_z) diagram of the premultiplied spanwise spectra of the turbulent kinetic energy $k_z E_{k_t}$($E_{k_t} = (E_{uu} + E_{vv} + E_{ww})/2$) and the scale-by-scale production $k_z P_{k_t}$, viscous dissipation $k_z \varepsilon_{k_t}$, viscous diffusion and pressure work $k_z D^{\nu}_{k_t} + k_z \Phi_{k_t}$, interscale transport $k_z T^{\mathrm{sc}}_{k_t}$, and spatial transport $k_z T^{\mathrm{sp}}_{k_t}$ obtained with the streamwise-minimal domain (the Lx-1.6 case). The values are scaled based on U_{w} and h.

viscous dissipation, pressure work, and viscous diffusion, which are respectively defined as:

$$P_{ij} = -E_{ik}\frac{\partial U_j}{\partial x_k} - E_{jk}\frac{\partial U_i}{\partial x_k}, \quad D^{\nu}_{ij} = \nu\frac{\partial^2 E_{ij}}{\partial x_k^2}, \tag{4}$$

$$\varepsilon_{ij} = 2\nu\left[\Re\left(\overline{\frac{\partial \hat{u}_i(k_z)}{\partial x}\frac{\partial \hat{u}_j(-k_z)}{\partial x}}\right)\right. \tag{5}$$

$$\left. + \Re\left(\overline{\frac{\partial \hat{u}_i(k_z)}{\partial y}\frac{\partial \hat{u}_j(-k_z)}{\partial y}}\right) - k_z^2 E_{ij}\right], \tag{6}$$

$$\Phi_{ij} = \frac{1}{\rho}\Re\left(\overline{\hat{u}_i(k_z)\frac{\partial \hat{p}(-k_z)}{\partial x_j}} + \overline{\hat{u}_j(k_z)\frac{\partial \hat{p}(-k_z)}{\partial x_i}}\right), \tag{7}$$

and N_{ij} is the nonlinear terms defined as:

$$\begin{aligned} N_{ij} = &-\Re\left(\overline{\widehat{u_i u}(k_z)\frac{\partial \hat{u}_j(-k_z)}{\partial x}} + \overline{\widehat{u_j u}(k_z)\frac{\partial \hat{u}_i(-k_z)}{\partial x}}\right) \\ &-\Re\left(\overline{\widehat{u_j v}(k_z)\frac{\partial \hat{u}_i(-k_z)}{\partial y}} + \overline{\widehat{u_j v}(k_z)\frac{\partial \hat{u}_i(-k_z)}{\partial y}}\right) \\ &-k_z\Im\left(\overline{\widehat{u_i w}(k_z)\hat{u}_j(-k_z)} + \overline{\widehat{u_j w}(k_z)\hat{u}_i(-k_z)}\right), \end{aligned} \tag{8}$$

where $\Im$ stands for the imaginary part of complex quantity. The nonlinear term N_{ij} represents the Reynolds-stress transport in both physical and scale space, and integrating this term for wavenumber yields the turbulent transport term:

$$\sum_{k_z} N_{ij} = -\frac{\partial \langle u_i u_j u_k \rangle}{\partial x_k}. \tag{9}$$

N_{ij} can be decomposed into the spatial transport $T^{\mathrm{sp}}_{ij}$and interscale transport T^{sc}_{ij}:

$$N_{ij} = T^{\mathrm{sp}}_{ij} + T^{\mathrm{sc}}_{ij}, \tag{10}$$

$$\text{where,} \quad \int_0^h T^{\mathrm{sp}}_{ij}\mathrm{d}y = 0, \quad \sum_{k_z} T^{\mathrm{sc}}_{ij} = 0. \tag{11}$$

Such decompositions can be done in mutiple ways (for example, Mizuno, 2016; Kawata & Alfredsson, 2018), and in the present study we define the spatial and interscale transports as:

$$\begin{aligned} T^{\mathrm{sp}}_{ij} = &\frac{1}{2}\frac{\partial}{\partial x_k}\left[\Re\left(\overline{\widehat{u_i u_k}(k_z)\hat{u}_j(-k_z)}\right)\right. \\ &\left. +\Re\left(\overline{\widehat{u_j u_k}(k_z)\hat{u}_i(-k_z)}\right)\right], \end{aligned} \tag{12}$$

$$T^{\mathrm{sp}}_{ij} = N_{ij} - T^{\mathrm{sc}}_{ij}, \tag{13}$$

similarly to the analysis by Mizuno (2016).

The spanwise spectra of the turbulent kinetic energy $E_{k_t} = (E_{uu} + E_{vv} + E_{ww})/2$ and the scale-by-scale budget of the transport equation is presented in Fig. 4. Such spectral energy budget has already been investigated in turbulent channel flow in some earlier studies in detail (e.g. Mizuno, 2016; Lee & Moser, 2019), and the present results show consistent tendencies in the behaviours of each term in the near-wall region: the turbulent energy is mainly generated by the production term P_{k_t} in the near wall region around $y^+ \approx 20$ at the spanwise wavelengths around $\lambda_z^+ \approx 100$, and most of the produced energy is directly dissipated by the viscous dissipation there or at smaller wavelengths after transferred by the interscale transport $T^{\mathrm{sc}}_{k_t}$. A part of the energy is transported to the channel central region or towards

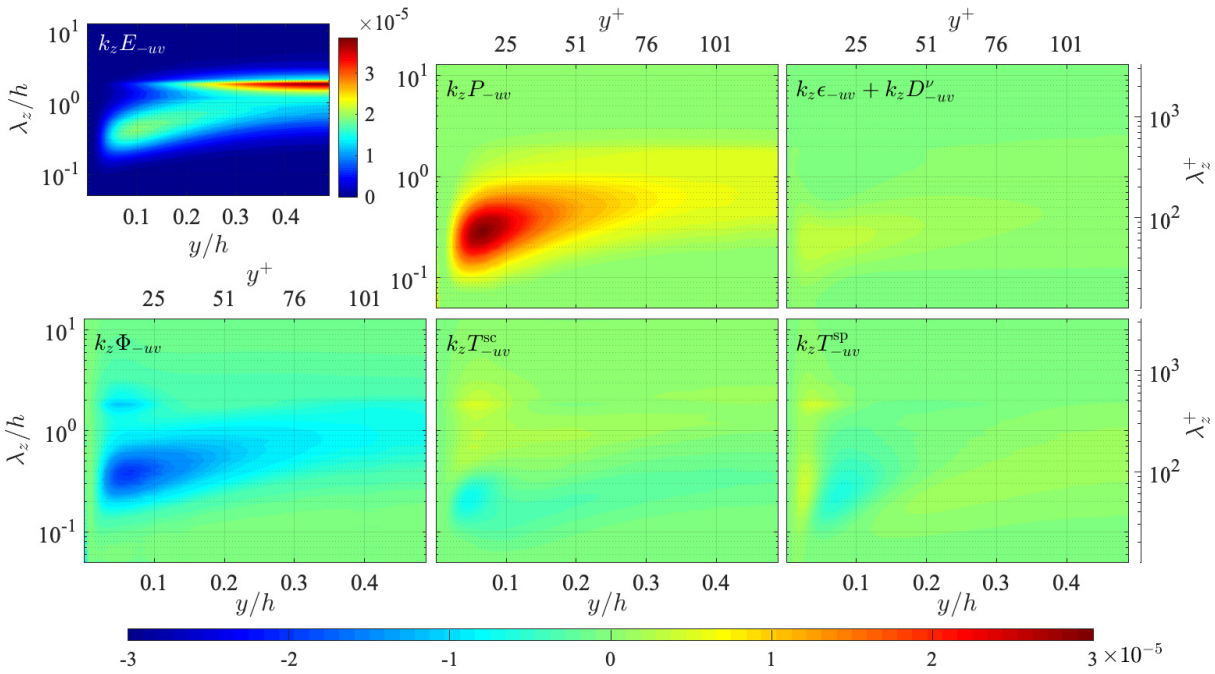

Figure 5. Space-wavelength (y-λ_z) diagram of the premultiplied spanwise cospectra of the Reynolds shear stress $k_z E_{-uv}$ and the scale-by-scale production $k_z P_{-uv}$, viscous dissipation and diffusion $k_z \varepsilon_{-uv} + k_z D^{\nu}_{-uv}$, pressure work $k_z \Phi_{-uv}$, interscale transport $k_z T^{sc}_{-uv}$, and spatial transport $k_z T^{sp}_{-uv}$ obtained with the streamwise-minimal domain (the Lx-1.6 case). These values are scaled based on U_w and h.

further wall vicinity by the spatial transport $T^{sp}_{k_t}$ and/or the viscous diffusion $D^{\nu}_{k_t}$ and dissipated there.

On the other hand, in the channel core region, the turbulent energy production is not zero in the plane Couette flow unlike in the channel flow due to the non-zero mean velocity gradient and the velocity fluctuations caused by the very-large-scale structure. One can see in Fig. 4 that the production spectra are weakly positive at relatively larger wavelengths in the channel core region, and the interscale transport transfers the energy towards the smaller scales, at which the energy is dissipated by the viscous dissipation. An interesting observation here is that the interscale transport $T^{sc}_{k_t}$ indicates a energy transport from smaller to larger wavelengths in the wall vicinity $y^+ \approx 8$, which may correspond to the near-wall reversed energy cascades observed, for example, by Saikrishnan *et al.* (2012) and Hamba (2018).

Figure 5 presents the space-wavelength diagram of the Reynolds shear stress cospectra E_{-uv} and the scale-by-scale budgets of the transport equation. As shown here, the cospectra distribution has the energy peaks in the near-wall and channel-core regions, and the production is significant at relatively small wavelengths in the near-wall region, similarly to those of the turbulent kinetic energy. The distinct difference of the Reynolds-shear-stress transport from that of the turbulent energy is that the interscale transport T^{sc}_{-uv} is shown to transfer the Reynolds shear stress from the smaller to larger wavelengths throughout the channel, unlike the turbulent energy interscale transport. Such inverse interscale transport of the Reynolds shear stress was also observed experimentally by Kawata & Alfredsson (2018).

The other characteristics of the Reynolds shear stress transport is that the viscous dissipation plays only very minor roles throughout the channel, unlike the budget of the turbulent energy, and it is the pressure-work Φ_{-uv} that instead dissipates the Reynolds stress. In Fig. 5, it is shown that the pressure-work spectra are negative at most wavelengths throughout the channel, as expected, and the negative region of Φ_{-uv} corresponds well to the positive regions of the productions P_{-uv} and the interscale transport T^{sc}_{-uv}.

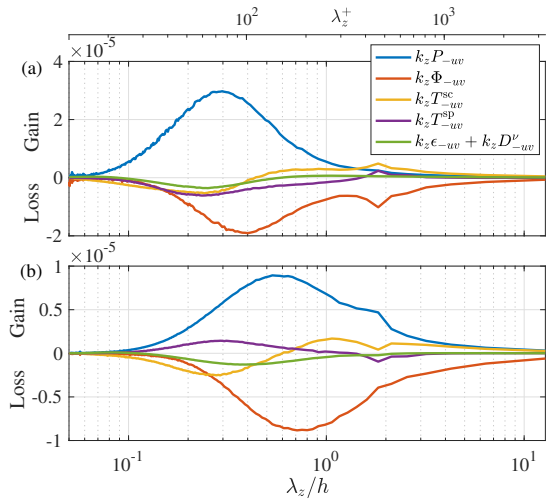

Figure 6. Scale-by-scale budget balance of the Reynolds shear stress transport at the wall-normal position (a) $y^+ = 18$ and (b) $y/h = 0.28$ ($y^+ = 72$) obtained with the streamwise-minimal domain (the Lx-1.6 case). These values are scaled based on U_w and h.

Figure 6 gives more detailed comparison of the spectral budget of the Reynolds shear stress transport at the wall-normal locations (a) in the inner layer $y^+ = 18$ and (b) in the logarithmic region $y/h = 0.28$ ($y^+ = 72$). As shown in Fig. 6(a), the production and the pressure-work contributions are dominant in the spectral budget balance in the

near-wall region. It is particularly noteworthy that the peak of the pressure work is located at larger wavelengths compared to the production, and such tendencies are also found in the logarithmic region as shown in Fig. 6(b). The magnitude of the interscale and spatial transports are relatively small compared to P_{-uv} and Φ_{-uv}, particularly in the near-wall region as shown in Fig. 6(a). Their contributions are, however, more than 15 % of the local level of P_{-uv}, and and more significant in the logarithmic region (see Fig. 6(b)). The viscous dissipation ε_{-uv} and diffusion D^{ν}_{-uv} are not significant at both wall-normal locations.

The profiles of the spectra budget of the Reynolds shear stress transport indicate that the Reynolds shear stress is produced at smaller scales and dissipated at larger scales by the effect of pressure after the inverse interscale transport by T^{sc}_{-uv} (and spatial transport by T^{sp}_{-uv}). This is totally different from the transport of the turbulent kinetic energy, where the energy is produced at larger scales, transferred towards smaller scales by the turbulent energy cascade, and eventually dissipated by viscosity at small scales.

CONCLUSION

In the present study, spectral budgets of the transport equation of the turbulent kinetic energy and the Reynolds shear stress have been investigated in the turbulent plane Couette flow by means of DNS. In order to reduce the computational cost, the computational domain size in the streamwise direction was reduced to as small as the minimal length, i.e. the least domain size to sustain the near-wall cycle, and the effect of reducing the domain size was examined. The computation with the streamwise-minimal domain reproduces fairly well the statistical characteristics of the plane Couette turbulence including the spectral contents, and the obtained spectral budget of the turbulent kinetic energy and the Reynolds shear stress showed consistent tendencies with the results by earlier studies. The roles of the interscale and spatial transport, which bring the Reynolds shear stress from relatively small scales near the wall to larger scales in the channel core region, are found significant in comparison to the contribution of the production by the mean flow. It is also revealed that viscosity does not play significant role in the Reynolds shear stress transport at any scale throughout the channel, and the Reynolds shear stress is dissipated by the effect of pressure at larger scales than those it is produced at, after the inverse interscale transfer. This is in contrast to the turbulent energy transport, where the energy is cascaded to smaller scales and dissipated by viscosity.

REFERENCES

Abe, Hi., Antonia, R. A. & Toh, S. 2018 Large-scale structures in a turbulent channel flow with a minimal streamwise flow unit. *J. Fluid Mech.* **850**, 733–768.

Avsarkisov, V., Hoyas, S., Oberlack, M. & García-Galache, J. P. 2015 Turbulent plane Couette flow at moderately high Reynolds number. *J. Fluid Mech.* **751-R1**.

Bech, K. H., Tillmark, N., Alfredsson, P. H. & Andersson, H. I. 1995 An investigation of turbuelnt plane Couette flow at low Reynolds numbers. *J. Fluid Mech.* **286**, 291–325.

Cimarelli, A., De Angelis, E., Jiménez, J. & Casciola, C. M. 2016 Cascades and wall-normal fluxes in turbulent channel flows. *J. Fluid Mech.* **796**, 417–436.

Dogan, E., Örlü, R., Gatti, D., Vinuesa, R. & Schlatter, P. 2018 Quantification of amplitude modulation in wall-bounded turbulence. *Fluid Dyn. Research* **To appear** (DOI: 10.1088/1873-7005/aaca81).

Hamba, F. 2018 Turbulent energy density in scale space for inhomogeneous turbulence. *J. Fluid Mech.* **842**, 532–553.

Hultmark, M., Vallikivi, M., Bailey, S. C. C. & Smits, A. J. 2012 Turbulent pipe flow at extreme reynolds numbers. *Phys. Rev. Lett.* **108**, 094501.

Hutchins, N. & Marusic, I. 2007 Large-scale influences in near-wall turbulence. *Phil. Trans. R. Soc. Lond. A* **365**, 647–664.

Jimenez, J. & Moin, P. 1991 The minimal flow unit in near-wall turbulence. *J. Fluid Mech.* **225**, 213–240.

Kawata, T. & Alfredsson, P. H. 2018 Inverse interscale transport of the Reynolds shear stress in plane Couette turbulence. *Phys. Rev. Lett.* **120**, 244501.

Komminaho, J., Lundbladh, A. & Johansson, A. V. 1996 Very large structures in plane turbulent Couette flow. *J. Fluid Mech.* **320**, 259–285.

Lee, M. & Moser, R. D. 2017 Role of large-scale motions in turbulent Poiseuille and Couette flows. In *Proc. 10th Symp. Turbulent Shear Flow Phenomena*. Swissotel, Chicago-IL, USA.

Lee, M. & Moser, R. D. 2019 Spectral analysis of the budget equation in turbulent channel flows at high Reynolds number. *J. Fluid Mech.* **860**, 886–938.

Lee, M. J. & Kim, J. 1991 The structure of turbulence in a simulated plane Couette flow. In *Eighth Symp. Turbulent Shear Flow*. Tech. University of Munich.

Mizuno, Y. 2016 Spectra of energy transport in turbulent channel flows for moderate Reynolds numbers. *J. Fluid Mech.* **805** (25), 171–187.

Saikrishnan, N., Angelis, E. De, Longmire, E. K., Marusic, I., Casciola, C. M. & Piva, R. 2012 Reynolds number effects on scale energy balance in wall turbulence. *Phys. Fluids* **24** (1), 015101.

Samie, M., Marusic, I., Hutchins, N., Fu, M. K., Fan, Y., Hultmark, M. & Smits, A. J. 2018 Fully resolved measurements of turbulent boundary layer flows up to Re_τ =20,000. *J. Fluid Mech.* **851**, 391–415.

Smits, A.J., McKeon, B.J. & Marusic, I. 2011 High–Reynolds number wall turbulence. *Annu. Rev. Fluid Mech.* **43** (1), 353–375.

Toh, S. & Itano, T. 2005 Interaction between a large-scale structure and near-wall structures in channel flow. *J. Fluid Mech.* **524** (10), 249–262.

Tsukahara, T., Kawamura, H. & Shingai, K. 2006 DNS of turbulent Couette flow with emphasis on the large-scale structure in the core region. *J. Turbul.* **7** (19).

Willert, C. E., Soria, J., Stanislas, M., Klinner, J., Amili, O., Eisfelder, M., Cuvier, C., Bellani, G., Fiorini, T. & Talamelli, A. 2017 Near-wall statistics of a turbulent pipe flow at shear Reynolds numbers up to 40 000. *J. Fluid Mech.* **826**, R5.